A THEORETICAL AND EXPERIMENTAL INVESTIGATION OF SECONDARY JETS IN A MACH 6 FREE STREAM WITH EMPHASIS ON THE STRUCTURE OF THE JET AND SEPARATION AHEAD OF THE JET

By James R. Sterrett and John B. Barber

NASA Langley Research Center
Langley Station, Hampton, Va., U.S.A.

Presented at the
Separated Flows Specialists Meeting
Fluid Dynamics Panel – AGARD

Brussels, Belguim
May 9-11, 1966

NATIONAL AERONAUTICS AND SPACE ADMINISTRATION

A THEORETICAL AND EXPERIMENTAL INVESTIGATION OF SECONDARY JETS IN A MACH 6 FREE STREAM WITH EMPHASIS ON THE STRUCTURE OF THE JET AND SEPARATION AHEAD OF THE JET

By James R. Sterrett* and John B. Barber*
NASA Langley Research Center

SUMMARY

An experimental and theoretical investigation to determine the actual fluid processes in the interaction of secondary gaseous jets with a primary flow has been conducted. The experimental phase of the program consisted of an investigation of free jets exhausting against a flat plate, including interferograms taken with a laser grating interferometer, and an investigation conducted in a Mach 6 wind tunnel with secondary jets of various exit Mach numbers issuing perpendicularly from a flat plate. The theoretical investigation included the calculation of various free jet patterns by the use of the two-dimensional characteristic theory for various boundary conditions and the examination of various shock calculations for different shock patterns. Since this is a problem area where separation plays a prominent role, an analogy between different types of separated flow is presented. From these studies, realistic flow models have been constructed and various design parameters have been determined experimentally.

Author

INTRODUCTION

Most envisioned controls for maneuverable hypersonic vehicles necessitate exposure of moving parts to the very high temperatures associated with hypersonic speeds. One type of control that does not have this particular problem is the secondary jet control. When operating within the atmosphere, the secondary jet produces an interaction force in addition to the reaction force by causing the primary airstream to separate from a portion of the vehicle, creating a high surface pressure in that region as shown in figure 1. Although a number of experimental and analytical investigations on secondary jets have been published (for example, refs. 1 to 10), the interaction processes are still not well understood. While an understanding of the processes involved is not solely a separation problem, it is a problem area where separation plays a prominent role. Therefore, an analogy between different types of separated flow is presented.

The approach to the problem of determining the flow process for secondary jets was to conduct both experimental and theoretical investigations. The

*Aerospace Engineer.

experimental phase of the program consisted of an investigation of underexpanded free jets exhausting against a flat plate and an investigation conducted in a Mach 6 wind tunnel with secondary jets issuing perpendicularly from a flat plate. The theoretical phase included the calculation of various free jet patterns by the use of the two-dimensional characteristic theory for various boundary conditions and the examination of various shock calculations for different shock patterns. The purpose of this paper is to present the results of these studies. This investigation, in addition to having a practical application for hypersonic controls, is of interest for studies concerned with thrust vector control of rocket motors and fuel injection for supersonic combustion.

SYMBOLS

A,B	regions surrounding jet (see fig. 4)
d	width of jet slot at throat, in. (m)
$C_{N,A}$	coefficient of integrated normal force per inch span due to aerodynamic interaction of jet, $\frac{\int_l (P - P_o)dx}{qL}$
$C_{N,R}$	coefficient of calculated normal force per inch span due to reaction of jet alone, $\frac{\text{Thrust}}{qL}$
h	height of jet strong shock, measured from jet exit, in. (m)
H	height of plate from jet exit, in. (m)
K, K_a, K_h, K_l	constants
l	length of separated region, in. (m)
L	length of plate from leading edge to step, wedge, or jet, in. (m)
M	Mach number
$\dot{m}$	mass flow parameter (eq. (3))
P	pressure, lb/in^2 abs (N/m^2)
q	dynamic pressure, lb/in^2 abs (N/m^2)
R	Reynolds number
T	temperature, ^oK

x,y	Cartesian coordinates (flow of jet at nozzle exit parallel to "y," free stream parallel to "x") origin at beginning of step, wedge or jet
1,2,3,4,5	various jet regions
α	separation angle, calculable from reference 13
δ	boundary-layer displacement thickness, in. (m)
Δ	flow deflection across a shock, degrees
θ	angle of plate relative to x-axis, degrees
ν	Prandtl-Meyer expansion angle, degrees
ρ	density, Kg/m^3

Subscripts:

b	boundary conditions
c	conditions along center line of jet
j	jet exit conditions
max	maximum
o	local conditions on plate with attached flow
p	peak, and calculated from pressure measurements
p,1	conditions at first peak pressure for turbulent separation (not connected with numerals designating jet regions)
p,2	conditions at second peak pressure for turbulent separation (not connected with numerals designating jet regions)
s	step
t,j	jet stagnation conditions
t,∞	free-stream stagnation conditions
1,2,3,4,5	conditions at various jet regions
∞	free-stream test section or ambient conditions

MODEL OF SEPARATED AND REATTACHING FLOWS

The so-called Chapman-Korst separation model (refs. 11 and 12) is generally accepted to give the qualitative features of hypersonic two-dimensional turbulent separated flow. Typically the separated flow region is characterized by a more or less constant pressure after separation followed by a rising pressure just before reattachment. At the separation point the velocity along the dividing streamline is zero, but because of mixing the velocity along the dividing streamline increases in the downstream direction. Under the dividing streamline there is a region of reverse flow (see sketch in fig. 2). When the flow reattaches, the velocity again goes to zero and the pressure increases. The actual mechanism of reattachment is very complex and is not well established. In the original model the stagnation pressure at reattachment was assumed to be equal to the final downstream static pressure, however, present indications are that the stagnation pressure at reattachment is largely influenced by conditions near the reattachment point. Some experimental indication of this from unpublished data are shown in figures 2 and 3(a). In figure 2 the pressures in front of and on the face of different height steps are shown. While the peak pressures in the separation region on the plate remain approximately constant with increasing step height (e.g., ref. 13), the pressures near the top of the face, where reattachment occurs, vary considerably. Though the exact position of reattachment is unknown, it is evident that either the pressure at reattachment varies with step height or the pressure at reattachment is not determined by the maximum pressure rise. In figure 3(a), where the pressures for wedge forced separation are shown, it can be seen that the pressure at reattachment is much below the overall pressure rise. The reattachment position was located by comparing the surface pressures with a surface probe's total pressures (corrected for shock total-pressure loss). Apparently the extreme mixing in the reattachment region allows the total pressure of the flow adjacent to the surface to change very rapidly and become equal to or greater than the downstream static pressure. At any rate, the pressures near reattachment vary rapidly and the reattachment process is an extremely complicated interaction between the viscous flow field, the external flow and the shock field (note that the shocks extend well into the mixing region).

When separation is forced by a jet, the separated flow field is very similar to that previously discussed, and the surface pressures associated with the jet separated flow exhibit similar trends (fig. 3(b)). The jet can be considered to form a fluid surface or interface between the jet flow and the primary flow, and the dividing streamline in the mainstream separation region must join a jet fluid streamline instead of joining the wall. With this general flow pattern in mind, the secondary jet structure including the interaction between the jet and primary airstream will now be examined.

THEORETICAL CALCULATIONS FOR FREE JETS

Characteristic calculations.- Flow patterns of two-dimensional free jets with various ambient pressure conditions and nozzle exit Mach numbers were

calculated by the use of the characteristic equations assuming no mixing along the boundaries. Sketches which show typical flow patterns and part of the coarse net characteristic network for nozzle exit Mach numbers of 1.0 and 3.24 are shown in figures 4(a) and 4(b). The pressure on both sides of the jet is sufficiently low that as the flow emerges from the jet nozzle exit it expands to a higher Mach number and expansion waves originate from both sides of the nozzle exit and propagate through the body of the jet. Some of these expansions intersect the opposite boundary of the jet, and reflect as compression waves. These compressions then propagate through the body of the jet, and gradually merge and coalesce into an oblique shock (labeled "internal shock" in fig. 4). A comparison of the network of figure 4(a) with figure 4(b) shows that for a given jet pressure ratio the strength of this internal shock increases much more rapidly for a sonic jet than for the supersonic exit nozzles. The pressure along the jet boundary is a constant and is equal to the ambient pressure in that region. While these characteristic calculations define the properties at any point within the jet, they do not determine how the jet flow terminates since this is a function of the back pressure (see refs. 14 and 15).

Figure 4 also shows Mach number contour lines. The maximum possible jet Mach number obtainable on the center line of the jet depends on the expansions originating at each side of the jet exit nozzle and is calculable from the known pressure ratios $P_A/P_{t,j}$ and $P_B/P_{t,j}$. The maximum possible Mach number can be calculated by the following equation using Prandtl-Meyer turning angle properties:

$$\nu_{max} = \nu_j + \left(\nu_A - \nu_j\right) + \left(\nu_B - \nu_j\right) = \nu_A + \nu_B - \nu_j \tag{1}$$

Figure 5 shows the center line Mach number distribution for a sonic jet $\left(M_j = 1.0\right)$ for several different pressure ratios. Any decrease in the pressure ratios $P_A/P_{t,j}$ and $P_B/P_{t,j}$ merely extends the center line Mach number to higher values without changing the already established center line Mach number distributions as long as $P_A/P_{t,j} = P_B/P_{t,j}$. If $P_B/P_{t,j}$ is less than $P_A/P_{t,j}$, the center line Mach number distribution remains the same for any particular exit nozzle Mach number until

$$\nu_c = 2\nu_A - \nu_j \tag{2}$$

The center line Mach numbers for various jet exit Mach numbers are presented in figure 6. This plot is valid as long as the center line Mach number does not exceed that given by equation (2). As can be seen from the figure, at any given distance from the plate, the Mach number on the center line decreases as the exit nozzle Mach number increases except in the region where the first expansion from the next nozzle has not reached the center line.

For a given gas the jet total pressure and the exterior pressure in region A and B of figure 4 determine the position of the side boundaries and the internal shock. Over much of the pressure range, the pressures in region B have no effect on the boundary streamline near the plate in region A. The sketch in figure 7 illustrates this fact by showing that the last expansion from point D for the pressure ratio of $P_B/P_{t,j} = 0.1$ does not intersect the boundary within figure limits and therefore does not affect the boundary streamline near the surface shown in region A. If the pressure in region B is decreased still further, the expansion fan from point D grows in size, but none of the additional expansions intersect or change the portion of the boundary streamline shown in region A from its previous location.

Jet boundaries for underexpanded sonic jets exposed to varying ambient pressures are presented in figure 8(a), showing the growth in jet size as the ratio of ambient pressure to jet total pressure is decreased. In figure 8(b) are shown boundaries of jets of varying exit Mach numbers exhausting into a pressure field similar to that occurring in actual secondary injection. In this case the jets all have the same throat width and therefore their exit widths differ. The spreading of the jet decreases as the jet Mach number increases due to the decrease of static pressure at the exit with increase of Mach number.

Triple point.- The initial structure of the jet used as the basis for the characteristic layouts is eventually terminated, at some distance from the jet orifice, through a shock pattern due to the influence of the back pressure and viscous mixing. While under certain conditions the flow in the central core can remain supersonic after passing through the shock pattern (ref. 15), the jets considered here are not of this type. The flow in the central core passes through a strong shock, referred to here as the jet strong shock (also called the "Mach disc shock") and becomes subsonic. This jet strong shock intersects the internal shock on either side of the jet center line, and a reflected shock is formed at this intersection that in turn intersects the outer boundary of the jet (see fig. 9(b)). Since this is a free boundary, expansion waves originate when the reflected shock intersect the boundary (also see ref. 14).

Flow conditions existing at the intersection of the jet strong shock, internal shock and reflected shock (the triple point) were investigated and the results are shown in the series of charts in figure 9. These charts are based on the conditions that the static pressures and flow directions in the adjacent regions 3 and 4, at the triple point, must be equal. In general, two different configurations at the triple point may exist. For a given value of Δ_{1-2}, Δ_{2-3} may be either clockwise (positive) or counterclockwise (negative), and figure 9(c) is for $\Delta_{2-3} > 0$ while figure 9(d) is for $\Delta_{2-3} < 0$. The charts were developed from oblique shock relations.

Use of figure 9 necessitates determination of M_1 and Δ_{1-2} at the triple point, and these quantities may be found from the characteristic calculations. Δ_{1-2} is the strength of the compressions that have coalesced to that

point to form the internal shock. Knowing M_1 and Δ_{1-2}, M_2 may be found from figure 9(a). This value of M_2, along with that of M_1, is then used to determine the remaining properties on the charts (Δ_{2-3}, Δ_{1-4}, and M_4). The only remaining problem is whether to use the set of charts for the positive or negative case of Δ_{2-3}. This may be determined by either examination of a photograph of the particular case or by knowledge of the configuration the flow passes through for the particular case in question. Noticeable from figures 9(c) and 9(d) is the fact that the jet strong shock at the triple point is not a normal shock ($\Delta_{1-4} = 0$) for the values of M_1 shown for $\Delta_{2-3} > 0$, and is normal only at a point for $\Delta_{2-3} < 0$ for a given M_1 value.

EXPERIMENTAL FREE JET STUDIES

In order to study experimentally a simple jet flow which is somewhat similar to the secondary injection process, two-dimensional sonic free jets exhausting against a flat plate were examined. The plate simulated to a certain degree the fluid interface between the jet and the primary stream flowing over it. Previous studies (e.g., ref. 16) of the interaction between a plate and free jet are instructive; however, interferograms obtained in the present investigation add much to the interpretation of the actual fluid processes. The interferograms were obtained by means of a laser-grating interferometer (ref. 17), adjusted such that each fringe represented a line of constant density. Pressure orifices along the plate provided surface pressure profiles. The jet orifice had a throat width of 0.054 inch (0.137 cm) and a span of 8 inches (20 cm), and exhausted into a partially evacuated chamber. The plate height "H" and plate angle "θ" were varied in order to change the back pressure and the boundary flow angles. In these studies only the shock pattern for a triple point intersection where $\Delta_{2-3} < 0$ (see fig. 9) were observed.

Typical plate pressure distributions and interferograms of the jet exhausting against a plate placed perpendicular to the flow of the center line of the jet ($\theta = 0^{\circ}$) are shown in figure 10 for a ratio of $P_{\infty}/P_{t,j} = 0.015$ and two different plate heights. The general structure of the jet (boundaries, internal shocks, slipstreams, jet strong shock, reflected shocks, and supersonic region after the reflected shock) can be identified and are shown in the simplified sketch of the flow field included in this figure. Simplified expansion and compression patterns which must exit in the supersonic stream immediately downstream of the reflected shock, and which play a large part in changing the flow direction, are also indicated in this sketch (not shown are the compression waves in the supersonic stream which have not coalesced into the internal shock and instead crossed the reflected shock).

In the central core of the jet, prior to the jet strong shock, the flow is isentropic and each fringe represents a line of constant Mach number, a few of which are shown in the interferograms. The flow on the jet center line, after passing through the jet strong shock, stagnates on the plate and then reexpands

to supersonic velocities on either side, as indicated by the Mach number distributions along the plate on the interferograms. These distributions were calculated assuming stagnation values equal to the stagnation condition on the plate above the jet center line.

As has previously been shown by other investigators, the center line stagnation pressure can be calculated from two-dimensional shock equations and the known Mach number distribution when the shock location is known. Values calculated by this method with measured shock locations are shown in figure 10(b) and agree reasonably well with the experimentally measured pressures. The following table shows values of the total pressures across the downstream face of the jet strong shock in figure 10 calculated by the same method.

H/d	x/d	$P_{t,5}/P_\infty$
9.3	0	8.15
	2.5	6.70
	4.5	5.76
18.6	0	4.27
	2.5	4.42
	4.5	3.82
	6.6	3.55

Since across the downstream face of the jet strong shock the flow has differing total pressures, a given fringe represents the indicated Mach number (see fig. 10(a)) only in the region immediately adjacent to the plate. The total pressure values in the table can be used to correct the Mach numbers shown in the figure for the flow that has passed through these points on the jet strong shock. For example, for the flow passing through the jet strong shock adjacent to the triple point ($x/d = 4.5$) when $H/d = 9.3$, the flow becomes sonic approximately where a fringe denoted by $M = 1.38$ at the plate would cross the slip line. The Mach number distributions in the free boundaries and in the supersonic region after the reflected shock are not shown in the interferograms as extreme mixing occurs in these regions, and while the density distributions are known the total pressures are not.

Calculations of the triple point conditions show that in order for the jet strong shock to be normal at the triple point for the case of $H/d = 9.3$ and $P_\infty/P_{t,j} = 0.015$, more than 20° of compression must have coalesced into the internal shock to that point (fig. 9). The characteristic calculations indicate that this number of compressions have not coalesced into the internal shock at the triple point location determined from the interferogram. Therefore, for this case the jet strong shock cannot be a normal shock at the triple point. Apparently, the range of solutions shown in the triple point charts (fig. 9) is attainable provided the back pressure is varied a sufficient amount.

It is reasonable to expect that the interaction between a primary airstream and a secondary jet could be better simulated by turning the plate such that it makes an angle with the jet ($\theta \neq 0^\circ$), since the primary stream must flow around the jet. When the plate is turned to a sufficiently large angle, the flow patterns near the plate are considerably different from those observed when the plate is at 0°. A typical interferogram and several plate pressure distributions for various plate angles and heights are shown in figures 11(b) and 11(c) for a value of $P_\infty/P_{t,j} = 0.024$ (the theoretical free jet boundaries and internal shocks calculated by the characteristic layouts are also indicated on the interferogram). The flow from the center of the jet no longer stagnates on the plate. Instead, the supersonic flow downstream of the reflected shock decelerates and stagnates on the plate as is indicated by the peak pressures, and the peak density ratios shown in the interferogram. Calculations based on triple point conditions (not shown) indicate that the flow emerging from the reflected shock has ample total pressure to yield the peak pressures shown even should it pass through a normal shock. This flow then expands to either side of the stagnation point and flows along the plate, as indicated by the sketch. Eventually, this stagnated flow from the reflected shock region, as well as the flow downstream of the jet strong shock, becomes supersonic, as is also indicated by the sketch. The pressure plot shows that a considerable difference exists between the pressure peaks for the plate at $\theta = 12^\circ$ and 35°; however, for a given plate angle, the peak pressure varies only slightly with a variation in plate height.

WIND-TUNNEL INVESTIGATION OF SECONDARY JETS

This section presents the results obtained by injecting air from a two-dimensional orifice located near the rear of a two-dimensional flat plate into a Mach 6 primary stream.* The parameters varied were secondary jet exit Mach number (1 to 6), slot width, jet total pressure, and end plates for the model. In addition to determining gross aerodynamic normal forces from pressure distributions, jet shock structure, jet penetration, and separation distances were examined. The experiments were carried out in the Langley 20-inch (0.5 m) hypersonic Mach 6 tunnel. A description of the tunnel is given in reference 13. The experiments were conducted with a constant free-stream unit Reynolds number of 6.5×10^6 per foot (21.3×10^6 per meter).

The basic model used in this program was a flat plate 10 inches wide (25 cm) with a 10° leading edge that tapered to a maximum radius of 0.001 inch (0.02 mm). The distance from the jet slot to the leading edge of the plate (L) was 19.25 inches (48.89 cm). Twenty-eight 0.06-inch (1.5 mm) diameter pressure orifices were installed along the center line of the plate, to measure surface pressures in the jet induced separation region. The jets, two dimensional, were formed by the back of the flat plate and interchangeable nozzle pieces. The sonic nozzle was adjustable, by means of inserting shims between the nozzle

*The authors wish to acknowledge the aid of Mr. David J. Romeo who was responsible for conducting many of the tests included in this section.

and flat plate at the ends of the jet slot. The jet slot had a span of 8 inches (20 cm). Supersonic nozzles were contoured and did not have adjustable throat widths. The test methods and technique and the model mount were similar to those of reference 4. It was found that the jet throat widths (d) tended to enlarge proportionally to the jet total pressure. Consequently, the deviations were calibrated and the corrected values of the jet throat width were used wherever this quantity appeared explicitly in a parameter or calculation.

Previous heat-transfer measurements taken in this same tunnel on a flat plate without a boundary-layer trip have shown that fully turbulent flow began at approximately a Reynolds number of 5×10^6 for conditions similar to the present tests. To increase the extent of the turbulent flow, boundary-layer trips with heights sufficient to move turbulent flow to the vicinity of the trip were added to the plate for the present tests. While boundary-layer profiles were not taken for the present test conditions, boundary-layer surveys taken on the plate with the trips under conditions where the free-stream Reynolds number was 26.2 percent higher than the present tests were available. Velocity profiles calculated from these surveys at two positions on the plate are presented in figure 12. These profiles also indicate that the boundary layer is turbulent.

Flow model.- When the flow from a secondary jet issues into a supersonic or hypersonic primary stream, it produces a very complex flow field. While it is difficult to describe the flow in minute detail, the gross aerodynamic structure of the flow can be established from considerations of separation, free jets, and the inspection of schlieren photographs taken of secondary jets exhausting into a primary stream. The schlieren photographs and sketch of figure 13 illustrates a typical flow pattern often observed when an underexpanded secondary jet interacts with a primary flow.

The basic structure of a secondary jet is identical to that of a free jet, as is indicated by the schlieren photographs of figures 3 and 13. For a given gas, the jet total pressure and the exterior pressures in regions A and B (of fig. 13) determine the position of the side boundaries and the internal shock on sides A and B, respectively. Conditions in the center core remain constant regardless of the exterior pressure. The flow in the center core passes through a strong shock and becomes subsonic while the flow along the side of the secondary jet passes through a reflected oblique shock and remains supersonic. The upstream portion of the supersonic fluid turns partially in an upstream direction as is shown by the sketch of figure 13. Somewhere in this "tongue of air" is a dividing streamline along which the fluid decelerates and forms a mutual stagnation point with the fluid along the dividing streamline located in the upstream separation region. All flow below these dividing streamlines turns back into the separated region. This behavior of part of the flow turning upstream is similar to that observed when a free jet exhausts against a flat plate placed at an angle to the jet center line (see fig. 11) except that the flow now meets a fluid boundary instead of a solid boundary. Of special interest are the separation regions upstream of the secondary jet and the distance that the secondary jet penetrates into the primary stream.

The effect of various design parameters on conditions in these regions will be discussed in the following sections.

Surface pressure distributions.- Figure 14(a) presents typical examples of the chordwise pressure distributions on the center line ahead of the jet position for varying jet total pressures. The schlieren photograph already presented in figure 3(b) along with a pressure distribution illustrates the position relationship between the flow patterns and the various pressure regions defined in that figure. The first peak pressure region is characteristic of that observed in a turbulent separation region. It is postulated that the second peak pressure is determined largely by the pressure at the mutual stagnation point along the dividing streamlines (assuming little mixing from the mutual stagnation point to the surface). The flow just below the dividing streamline is turned toward the surface and decelerated.

Increasing the jet total pressure ratio for any particular slot for a sonic jet causes a growth in the extent of the separation regions shown in figure 14(a); however, the shape of the pressure distribution remains very similar in appearance for all slot widths and jet total pressure ratios. Pressure distributions for various jet exit Mach numbers also shows that these distributions are similar in shape to those observed with a sonic jet. See figure 14(b) for a typical example.

A plot which shows the first peak pressures for various slot widths and jet exit Mach numbers is presented in figure 15. The peak pressures are reasonably well correlated when plotted as a function of the parameter $\left(P_{t,j}/P_{t,\infty}\right)\frac{d}{L}$. This parameter is an indication of the jet mass flow when $P_{t,\infty}$ is constant since

$$\dot{m} = \frac{0.01652}{\sqrt{T_{t,j}}}\left(P_{t,\infty}\right)\left(\frac{P_{t,j}}{P_{t,\infty}}\right)\left(\frac{d}{L}\right)L = K\,\frac{P_{t,j}}{P_{t,\infty}}\,\frac{d}{L} \tag{3}$$

The figure shows that the first peak pressures are essentially independent of jet exit Mach number and slot width, but increase slightly when the mass flow parameter $\left(P_{t,j}/P_{t,\infty}\right)\frac{d}{L}$ increases. The second peak pressures increase slightly as the mass flow is increased, although they seem to decrease very slightly with an increase in the exit Mach number.

Although the data is not presented the surface pressures downstream of the secondary jet are less than primary stream conditions as would be expected since the primary flow expands around the jet in a manner somewhat similar to that on the afterbody of a model.

Other secondary jet characteristics for sonic jets.- Three prominent phenomena associated with secondary injection are the jet strong shock height (an indication of the height of penetration of the jet into the primary stream), separation distance and the aerodynamic force due to interaction between the

jet and primary stream. Data of these three phenomena are plotted for comparison in figure 17 against the mass flow parameter. The plots have been made nondimensional by dividing the parameters by the plate length and by presenting the aerodynamic interaction force in coefficient form $\left(C_{N,A}\right)$. Included with the $C_{N,A}$ curve is a plot of the jet reaction force coefficient $C_{N,R}$.

As can be seen from figure 17, on logarithmic scales the curves of h/L, l/L, and $C_{N,A}$ are nominally straight-line functions of the jet mass flow parameter whose slopes are approximately equal; therefore, the following relations may be written:

$$\frac{l}{L} = K_l\left(\frac{P_{t,j}{}^d}{P_{t,\infty}L}\right)^a = K_l'\dot{m}^a \tag{4}$$

$$\frac{h}{L} = K_h\left(\frac{P_{t,j}{}^d}{P_{t,\infty}L}\right)^b = K_h'\dot{m}^b \tag{5}$$

$$C_{N,A} = K_a\left(\frac{P_{t,j}{}^d}{P_{t,\infty}L}\right)^c = K_a'\dot{m}^c \tag{6}$$

In this case, $a \approx b \approx 0.6$ and $c \approx 0.7$.

Length of the separated region was taken as the distance from the upstream nozzle wall of the jet to the point where the pressure on the plate surface was nominally equal to the surface pressure without the jet (see fig. 3(b)). It was found from schlieren photographs that the separation point, determined in this manner, coincided approximately with the point of impingement of the separation shock, if extended, on the plate. Previous separation work (refs. 11 and 13) has shown, by oil film techniques, that the actual point of separation lies slightly farther downstream than the position used here, and occurs at a position about halfway up the first pressure rise. No such techniques were used here; however, the method used here of determining a "hypothetical" separation point fits the purpose of this report adequately.

The jet strong shock heights were measured from schlieren photographs of the flow. An actual measurement of the height of jet penetration into the primary stream was not possible because the contact surface between the two flows was generally not discernible from the schlieren photographs. The scatter in the strong shock height data is due to difficulty in measuring the exact height of the shock from the photographs since the shock appeared as a "band." The height from the plate to the top and bottom of the shock "band" was measured and plotted. It might be expected that the plots of h/L and l/L versus jet mass flow would be similar, since the separation angle for turbulent separation is nearly a constant for a given free-stream Mach number, and the

separation lengths are nominally proportional, by geometry, to the height of the disturbance.

Shown in figure 18 is a plot of the static pressures above the jet strong shock plotted against the jet mass-flow parameter. The pressures were determined on the center line of the jet, and were found by using measured shock heights (h) from schlieren photographs and the known center line Mach number distribution (fig. 6), and assuming a normal shock at the center line. The normal shock condition is not too restrictive since the pressure ratio across a strong shock is rather insensitive to the shock angle. It can be seen that the pressure increases with jet mass flow.

Aerodynamic normal forces due to the interaction between the jet and primary flow over the plate were obtained by mechanical integration of the plate pressure-distribution curves. These forces were calculated ahead of the jet only and the results do not include the effects of the low pressure region behind the jet where the pressures are generally less than primary stream conditions. Also, the pressures used to determine these forces were obtained along the center line of the plate and therefore do not include the three-dimensional effects occurring near the plate edges.

It has been noted previously that the ratio of normal aerodynamic interaction force to jet reaction force decreases as the jet throat width increases (ref. 4) and as the ratio of jet total pressure to free stream total pressure increases (refs. 2, 5, and 8). These trends are shown for the present data in figure 19 where the aerodynamic to jet force ratios are plotted in coefficient form both against $P_{t,j}/P_{t,\infty}$ and the mass-flow parameter $\left(P_{t,j}/P_{t,\infty}\right)\frac{d}{L}$. These trends are a result of the fact that $C_{N,A}$ increases less than linearly with mass flow while $C_{N,R}$ increases linearly with mass flow (see fig. 17). The increase in jet mass flow can be caused by increasing the jet total pressure and/or increasing the jet throat width, thereby causing $C_{N,A}/C_{N,R}$ to decrease either as jet total pressure or throat width increases. However, the force ratio remains approximately constant for any given mass flow, regardless of slot width or jet pressure ratio. The exact cause for the data scatter of the 0.007 inch (0.0178 cm) throat width cases in figures 19(a) and 19(b) is unknown; however, any inaccuracy in the throat width calibration would have the greatest effect with the smallest throat width.

Included in figure 19(b) is a fairing of unpublished data by Staylor and Barber, wherein secondary injection through a two-dimensional slot from the base of 9° half angle cone was tested. The trends shown for this three-dimensional configuration are the same as those observed for the two-dimensional model reported here. However, the actual values of $\left(C_{N,A}/C_{N,R}\right)$ are less for the three-dimensional cone than for the two-dimensional flat plate, as might be expected by the results of reference 18. Data using helium as an injection also obtained by Staylor and Barber, shows that helium for a given mass flow gives greater values of $C_{N,A}/C_{N,R}$ than does air.

The normal force values given in reference 4 are believed to be somewhat in error due to the deflection of the plate forming the jet slot. The width of the slot in reference 4 was not measured under pressurized conditions. The percentage of error increased in all probability as the jet pressure was increased and as the normal slot width was decreased. However, the conclusion reached in reference 4 that the aerodynamic to reaction force ratio increases with decreasing jet throat width at a given jet pressure ratio remains in agreement with the results presented here.

The method employed to determine the aerodynamic interaction forces assumed the absence of any three-dimensional-flow effects. However, three-dimensional effects do exist near the edges of the jet, as shown by reference 18. To investigate the possibility that these three-dimensional effects were penetrating to the center line of the plate and affecting the measured surface pressures (and, consequently, the aerodynamic interaction forces), several runs were made with side plates on the model to make the flow more nearly two dimensional. Although only a small part of the data are presented in this paper (see fig. 17), the results show that the addition of side plates had an extremely small influence on the aerodynamic interaction force coefficients.

Supersonic secondary jet characteristics.- Values of $C_{N,A}$ for jets of various exit Mach numbers are shown plotted against the jet mass-flow parameter in figure 20. Also on these figures are solid lines indicating the calculated jet reaction force coefficients $\left(C_{N,R}\right)$ for the various jet Mach numbers. From these figures it is apparent that, for a given jet mass flow, the aerodynamic interaction force decreases and the jet reaction force increases as the jet exit Mach number increases. A comparison of the data for the Mach 3.2 jets shows that the jet mass-flow parameter correlates values of $C_{N,A}$ reasonably well for different jet throat widths for the supersonic jets, as well as for the sonic jets.

In figures 21, values of the total normal force $\left(C_{N,A} + C_{N,R}\right)$ are plotted against the mass-flow parameter. This figure shows that, although at a given jet mass flow $C_{N,A}$ decreases and $C_{N,R}$ increases as M_j increases, the sum of $C_{N,A}$ and $C_{N,R}$ remains nominally a constant for a given jet mass flow regardless of the jet exit Mach number. Therefore, under the conditions of this test program, a given jet mass flow produces a given total amount of force, regardless of how this force is divided into the reaction and aerodynamic interaction components.

Remarks concerning theoretical calculations.- A realistic flow model for underexpanded secondary jets issuing into a primary stream has been constructed, and from separation studies the first peak pressure $\left(P_{p,1}\right)$ in the separation region ahead of the jet exit can be estimated. Many of the other parameters involved in the interaction process can be reasonably well determined theoretically from separation and free jet considerations if the pressure in the region immediately downstream of the jet strong shock $\left(P_5 \text{ in fig. } 18\right)$ can be determined.

An example which illustrates how the aerodynamic normal-force coefficient can be estimated if P_5 is known is given below.

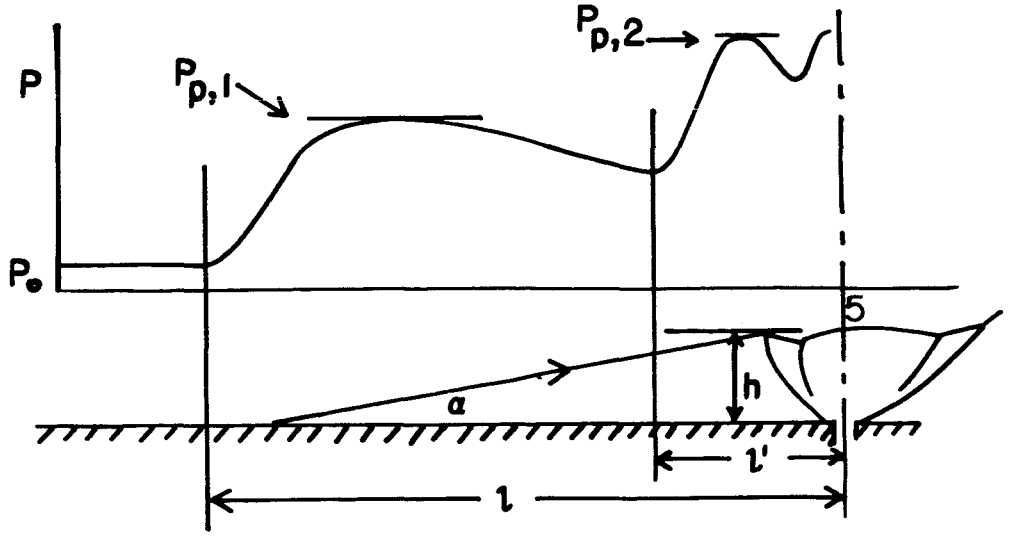

When the flow model is simplified as shown in the above sketch, the following equations may be written:

$$C_{N,A} = \frac{F_{N,A}}{qL} = \frac{\int_l (P - P_o)dx}{qL} \cong \frac{(l - l')P_{p,1} + l'P_{p,2}}{qL} \tag{7}$$

Since the values of $P_{p,1}$ and $P_{p,2}$ are known to be of the same magnitude and it is known that l' is appreciably less than l, and setting $l = \frac{h}{\tan \alpha}$ equation (7) may be rewritten as

$$C_{N,A} \cong \frac{lP_{p,1}}{qL} \cong \frac{hP_{p,1}}{qL \tan \alpha} \tag{8}$$

Since the required center line Mach number is given by

$$M_c = f(P_5, P_{t,j}) \tag{9}$$

and h is known for a given M_c as shown in figure 6, equation (8) can be solved for a given $P_{t,j}$ if P_5 is known. Calculated values of $C_{N,A}$ and $C_{N,R}$ are shown in figure 21, where $C_{N,A}$ was calculated from equations (8) and (9) and where P_5 is assumed to be either equal to $P_{p,1}$ or the values in figure 18. When the values of P_5 are taken from figure 18, these equations

predict reasonably well the experimental results. Perhaps a theoretical prediction of values of P_5 might be determined from momentum considerations as was done for an analogous situation in reference 19. However, the boundary conditions in the present case are not as well established as are those of reference 19. Secondary injection is a very complex problem involving interrelated phenomena and although equations (7) and (8) are not the result of a rigorous approach, they do not contain the rather severe simplications present in many previous analyses.

CONCLUDING REMARKS

An experimental and theoretical investigation to determine the actual fluid processes for secondary jet injection has been conducted. A realistic flow model was established from considerations of separation, free jet flow, and the actual interaction of secondary jets with a hypersonic mainstream. In general, the structure of the secondary jet is very similar to that of a free jet. The jet flow terminates by going through a complex shock system which allows part of the flow to go in an upstream direction. The magnitude of the surface pressures ahead of the jet exit position can be largely determined from boundary-layer separation considerations. However, the extent of the separation region is determined by the jet penetration height, an indication of which was obtained from measurements of the jet strong-shock standoff distance from the plate surface. The jet strong-shock standoff distances, pressure after this shock, separation distances and aerodynamic normal forces for the sonic jet with various slot widths can be correlated with the use of a jet mass-flow parameter. All of the parameters increase nonlinearly with increasing jet mass flow, making their direct scaling difficult. The ratio of the aerodynamic normal force $\left(C_{N,A}\right)$ divided by the reaction normal force $\left(C_{N,R}\right)$ increases with decreasing jet mass flow. Therefore the force ratio will increase as either slot width or jet total pressure is decreased. However, the force ratio remains approximately constant for any given jet mass flow, regardless of slot width or jet pressure ratio. The aerodynamic normal force for a given jet mass flow decreases with increasing jet exit Mach number, but the total normal force (including reaction) is approximately constant for a given jet mass flow and independent of jet exit Mach number for a given primary flow condition.

REFERENCES

1. Morkovin, M. V.; Pierce, C. A.; and Craven, C. E.: Interaction of a Side Jet With a Supersonic Main Stream. Bull. No. 35, Engineering Research Institute, University of Michigan, September 1952.

2. Vinson, P. W.; Amick, J. L.; and Liepman, H. P.: Interaction Effects Produced by Jet Exhausting Laterally Near Base of Ogive-Cylinder Model in Supersonic Main Stream. NASA MEMO 12-5-58W, 1959.

3. Ferrari, Carlo: Interference Between a Jet Issuing Laterally From a Body and the Enveloping Supersonic Stream. NASA N-74756, Bumblebee Rep. No. 286 (Contract NOrd 7386), Applied Physics Lab., John Hopkins University, April 1959.

4. Romeo, David J.; and Sterrett, James R.: Aerodynamic Interaction Effects Ahead of a Sonic Jet Exhausting Perpendicularly From a Flat Plate Into a Mach Number 6 Free Stream. NASA TN D-743, 1961.

5. Broadwell, James E.: Correlation of Rocket Nozzle Gas Injection Data. AIAA Journal, Vol. 1, No. 8, August 1963, pp. 1911-1913.

6. Strike, W. T.; Schueler, C. J.; and Deitering, J. S.: Interaction Produced by Sonic Lateral Jets Located on Surfaces in a Supersonic Stream. AEDC-TD-R-63-22, April 1963.

7. Charwat, A. F.; and Allegre, J.: Interaction of a Supersonic Stream and a Transverse Supersonic Jet. AIAA Journal, Vol. 2, No. 11, November 1964.

8. McDonald, R. D.; and Vinson, P. W.: A Study of Three Hypersonic Missile Control Devices. Research Report CR3978, Martin Company, Orlando Division, June 1964.

9. Mitchell, John W.: An Analytical Study of Two-Dimensional Flow Field Associated With Sonic Secondary Injection Into a Supersonic Stream. Vidya Technical Note 9166-TN-2, March 1964.

10. Kaufman, Louis G., II.: Classification of Interactions Due to High Speed Flows Past Transverse Jets. Research Report, Grumman Aircraft Engineering Corporation Research Department, Research Report RE-154, February 1962.

11. Chapman, Dean R.; Kuehm, Donald M.; and Larson, Howard K.: Investigation of Separated Flow in Supersonic and Subsonic Streams With Emphasis on the Effect of Transition. NACA Rep. 1356, 1958. (Supersedes NACA TN 3869.)

12. Korst, H. H.; Chow, W. L.; and Zumwalt, G. W.: Research on Transonic and Supersonic Flow of a Real Fluid at Abrupt Increases in Cross Section. University of Illinois M. E. Technical Report 392-5 (December 1959).

13. Sterrett, James R.; and Emery, James C.: Extension of Boundary-Layer-Separation Criteria to a Mach Number of 6.5 by Utilizing Flat Plates With Forward-Facing Steps. NASA TN D-618, 1960.

14. Adamson, Thomas C., Jr.: The Structure of the Rocket Exhaust Plume Without Reaction at Various Altitudes. Supersonic Flow, Chemical Processes and Radiative Transfer, Edited by D. B. Olfe, and V. Zakkay, Pergamon Press, Oxford, 1964.

15. Love, E. S.; Grigsby, C. E.; Lee, L. P.; and Woodley, M. J.: Experimental and Theoretical Studies of Axisymmetric Free Jets. NASA TR R-6 (1959).

16. Vick, A. R.; Cubbage, J. M.; and Andrews, E. H., Jr.: Rocket Exhaust Plume Problems and Some Recent Related Research. Specialists' Meeting on the Fluid Dynamic Aspects of Space Flight. Fluid Dynamic Panel of AGARD, Marseille, France (April 20-24, 1964), AGARDograph 87, vol. 2.

17. Sterrett, J. R.; Emery, J. C.; and Barber, J. B.: A Laser Grating Interferometer. AIAA Journal, vol. 3, no. 5, p. 963, May 1965.

18. Romeo, David J.: Aerodynamic Interaction Effects Ahead of Rectangular Sonic Jets Exhausting Perpendicularly From a Flat Plate Onto a Mach 6 Free Stream. NASA TN D-1800, 1963.

19. Romeo, David J.; and Sterrett, James R.: Flow Field For Sonic Jet Exhausting Counter to a Hypersonic Mainstream. AIAA Journal, vol. 3, no. 3, p. 544, March 1965.

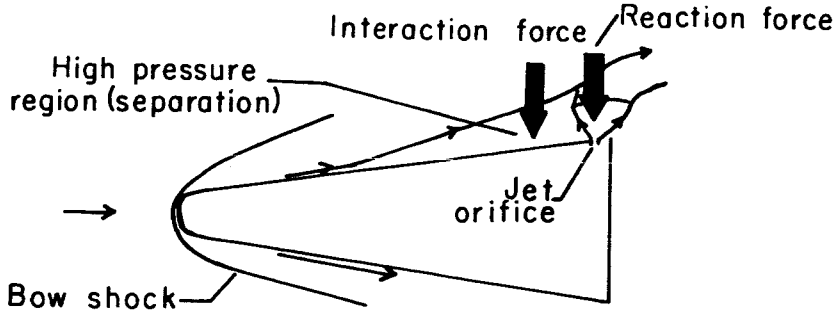

Fig. 1 Jet controlled hypersonic vehicle.

(a) Schlieren photograph.

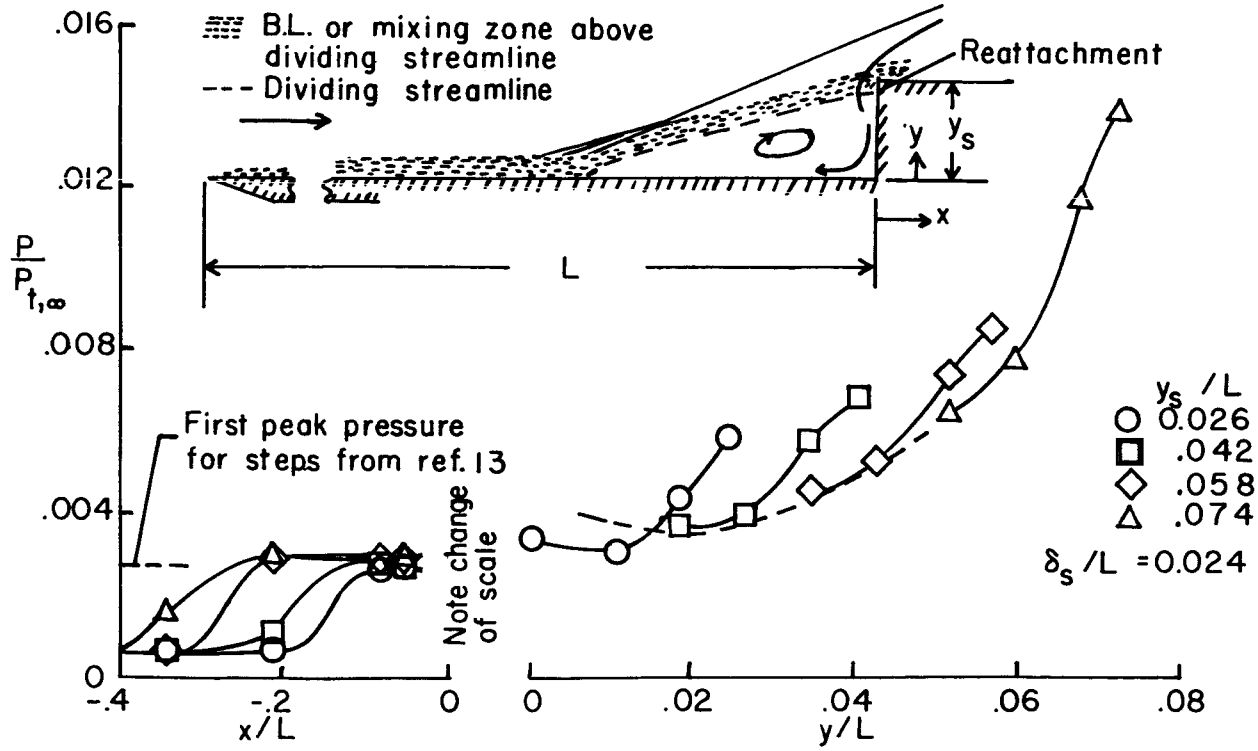

(b) Pressure distributions for various height steps and flow model.

Fig. 2 Turbulent separation on a flat plate forced by a forward facing step, $M_\infty = 6.0$, $R_\infty/ft = 8.4 \times 10^6$, L = 15.5 inches (39.37 cm.).

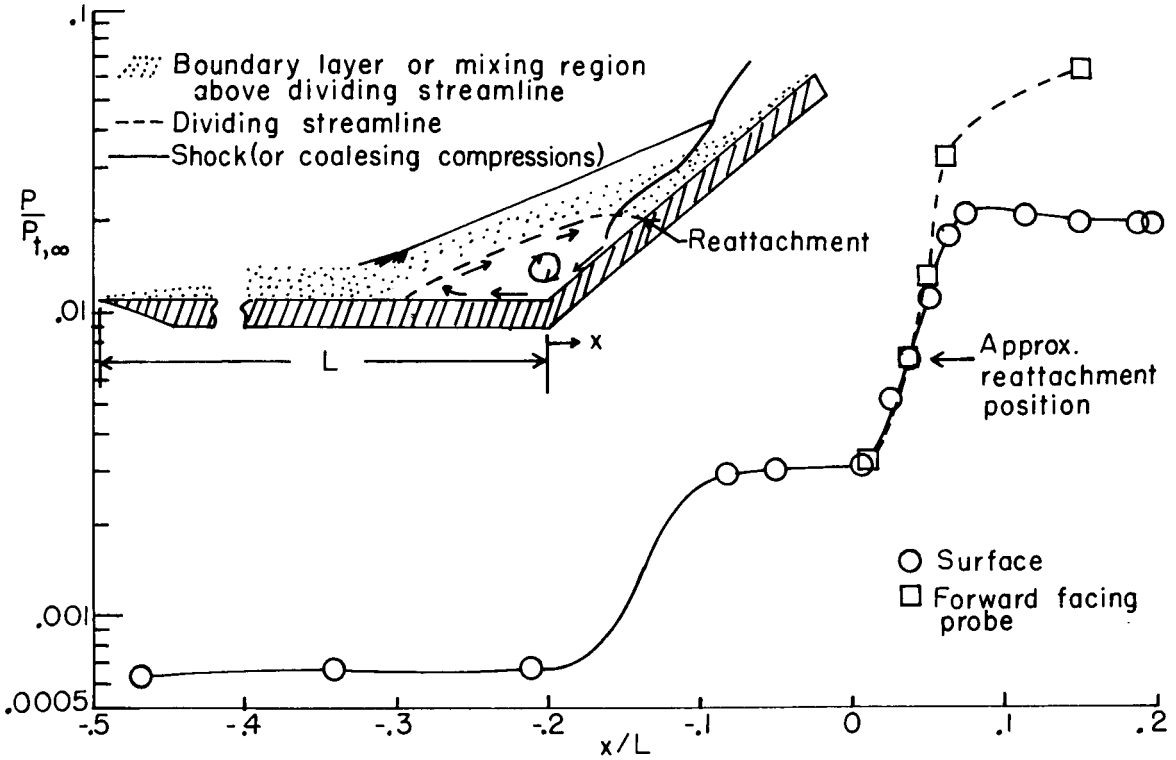

(a) Pressure distribution and flow model for 40° wedge $R_{\infty}/ft = 8.4 \times 10^6$, L = 15.5 inches (39.37 cm.).

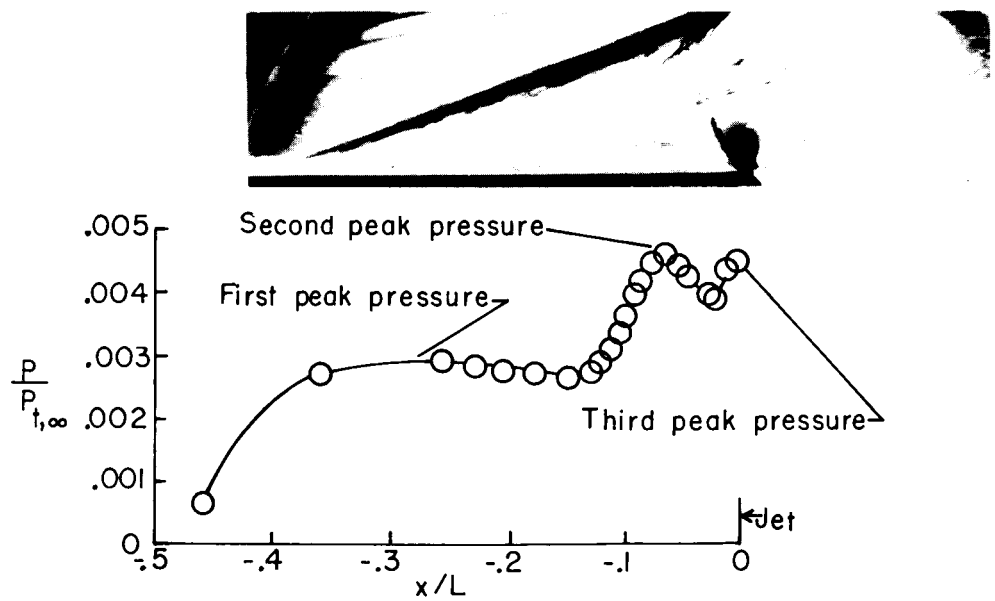

(b) Schlieren photograph and pressure distribution for secondary jet-induced separation. L = 19.25 inches (48.49 cm.), $M_j = 1.0$, d = 0.054 inches (0.137 cm) $P_{t,j}/P_{t,\infty} = 0.34$, $R_{\infty}/ft = 6.5 \times 10^6$.

Fig. 3 Turbulent separation on a flat plate forced by a wedge and a secondary jet, $M_{\infty} = 6.0$.

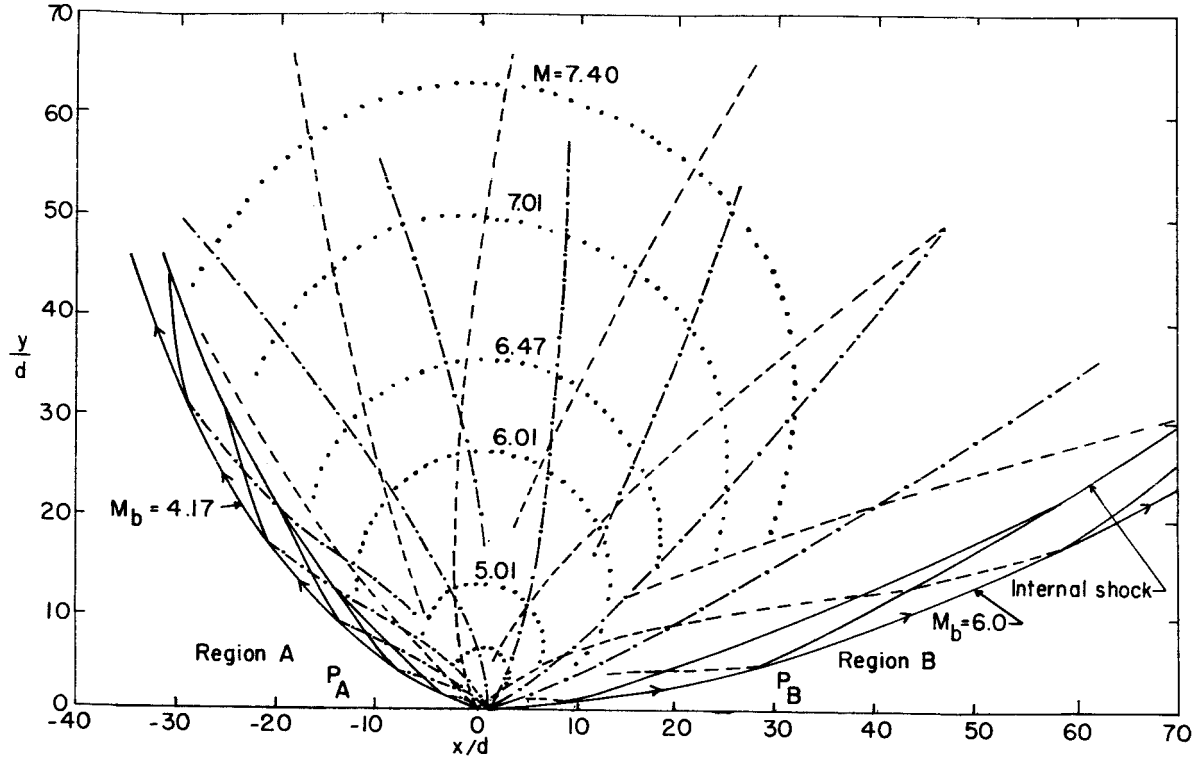

(a) M_j = 1.0.

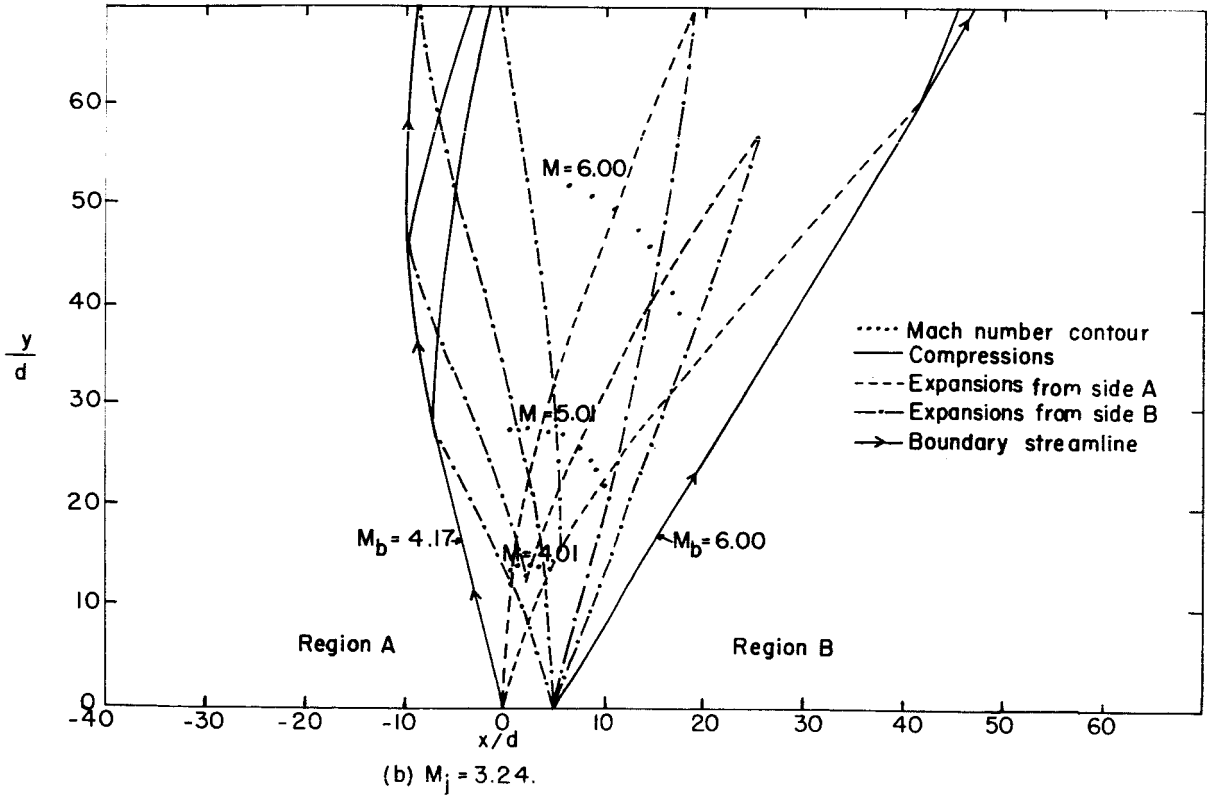

(b) M_j = 3.24.

Fig. 4 Typical characteristic layouts of free jets, $P_A/P_{t,j}$ = 0.00524, $P_B/P_{t,j}$ = 0.000629.

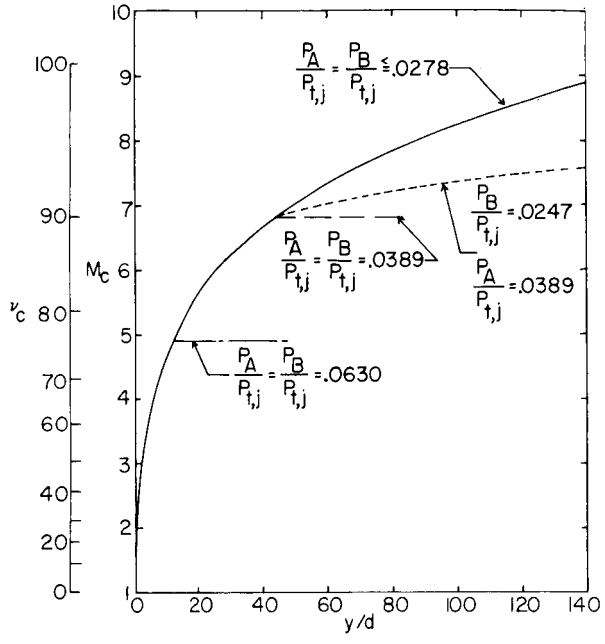

Fig. 5 Centerline Mach number distribution of a two-dimensional sonic jet for several different pressure ratios.

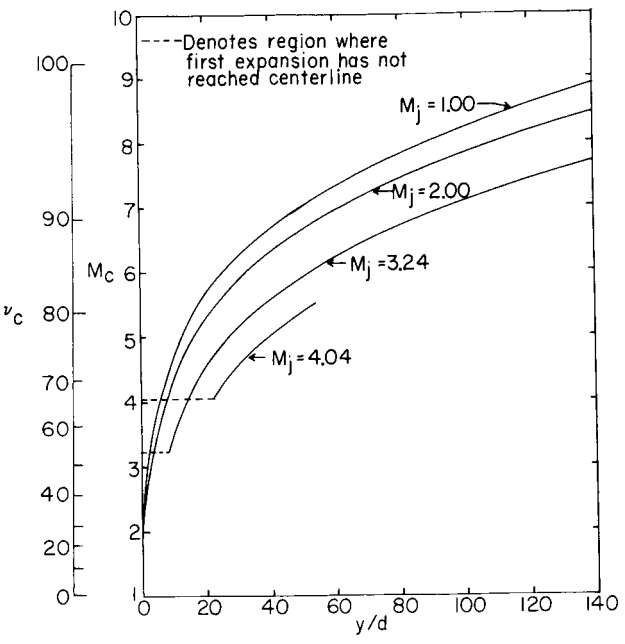

Fig.6 Theoretical Mach numbers along centerline for various jet exit Mach numbers.

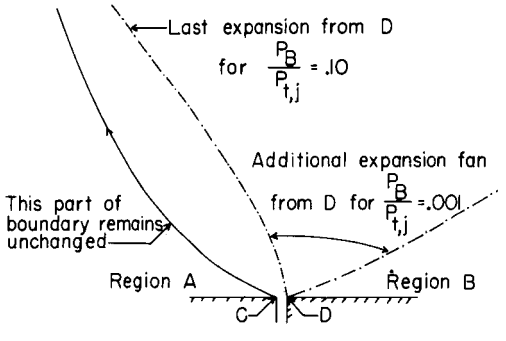

Fig.7 Effect of varying pressures in region B on boundary streamline in region A for $P_A/P_{t,j} = 0.005$.

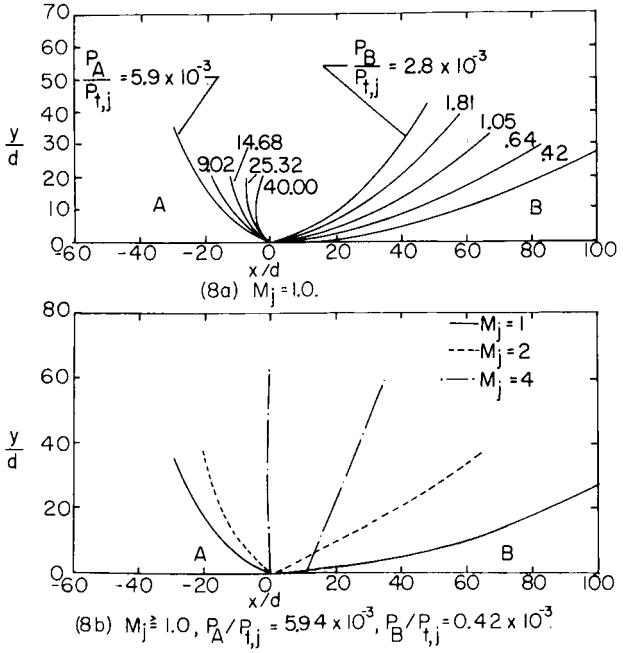

(8a) $M_j = 1.0$.

(8b) $M_j \geq 1.0$, $P_A/P_{t,j} = 5.94 \times 10^{-3}$, $P_B/P_{t,j} = 0.42 \times 10^{-3}$

Fig. 8 Two-dimensional jet boundaries.

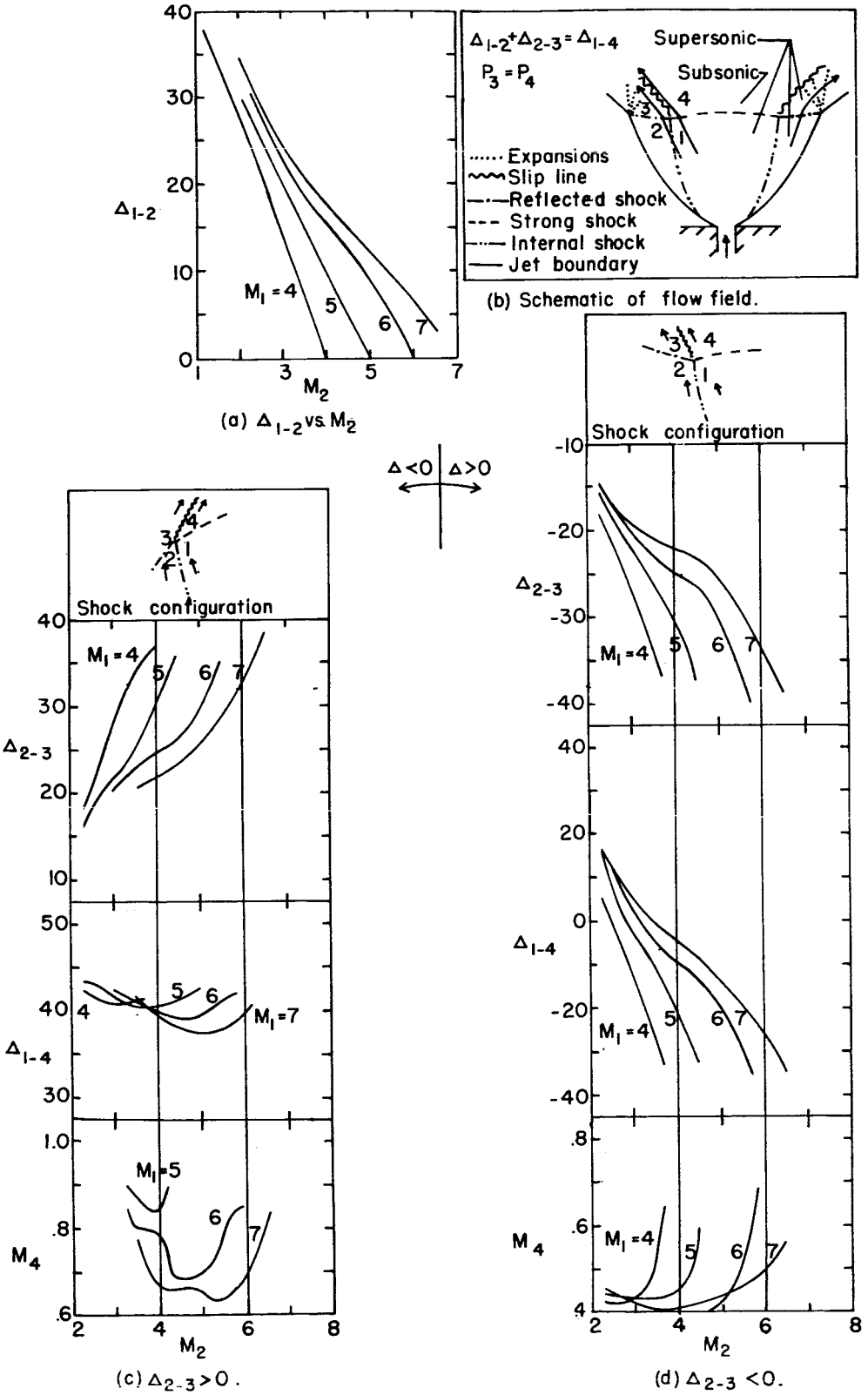

Fig. 9 Triple point shock calculations.

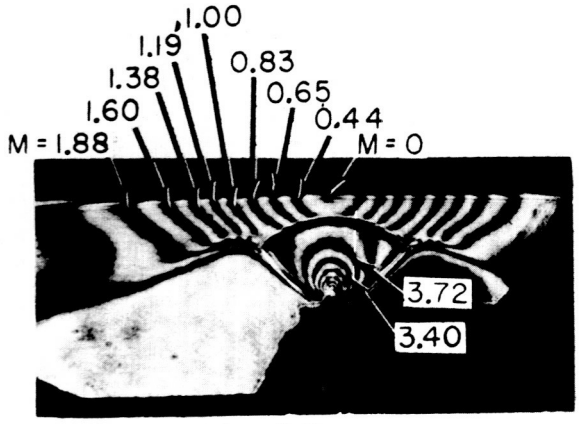

H/d = 9.3

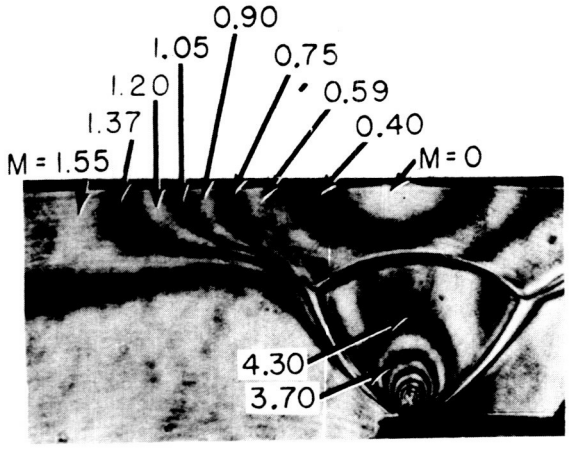

H/d = 18.6

(a) Mach number distributions along plates based on interferograms. $P_\infty / P_{t,j} = 0.015$.

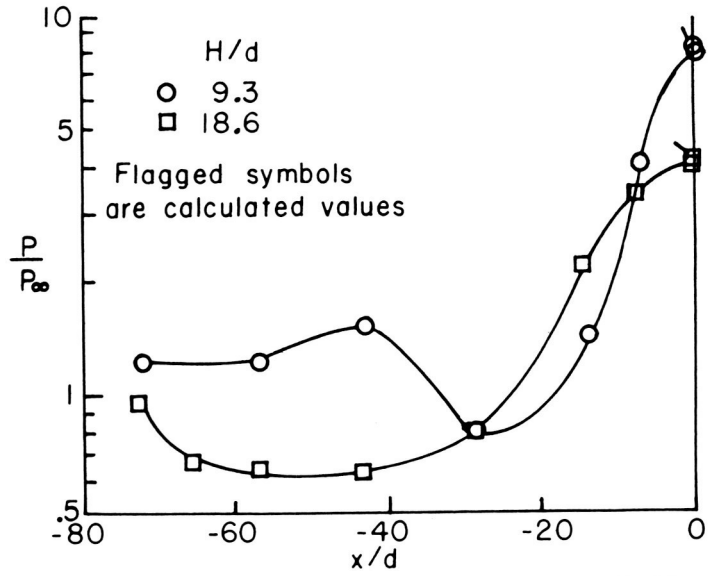

(b) Plate surface pressure distributions, $P_\infty / P_{t,j} = 0.015$.

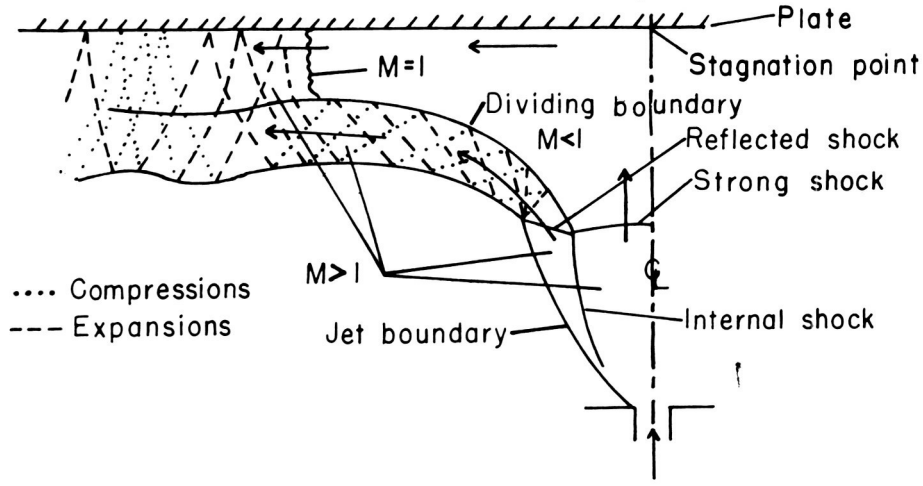

(c) Simplified sketch of flow field.

Fig. 10 Characteristics of jet exhausting against flat plate, $\theta = 0°$, $M_j = 1.0$.

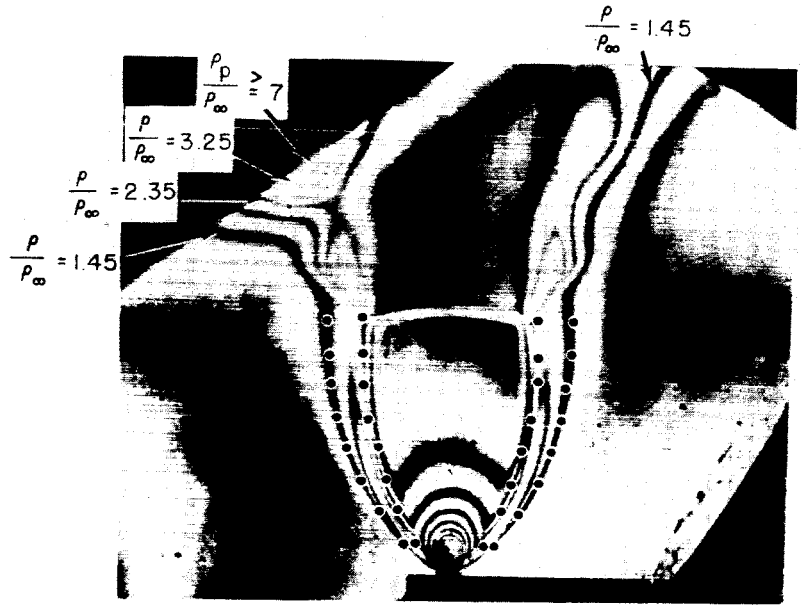

(a) Interferogram of jet with theoretical boundaries and internal shocks superimposed. $\theta = 35°$, $P_\infty / P_{t,j} = 0.024$, $H/d = 32.4$.

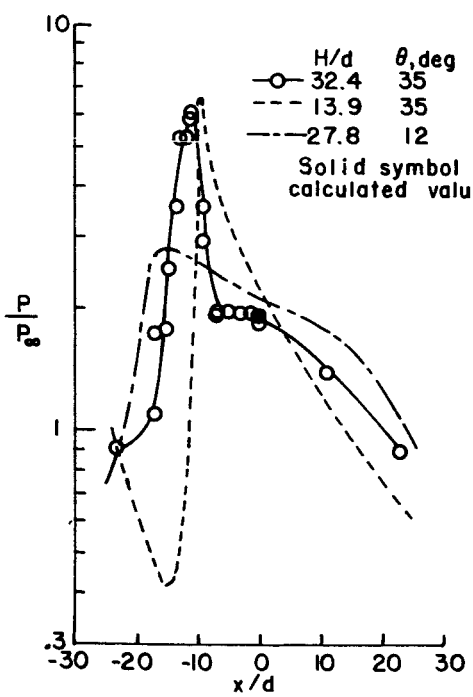

(b) Plate surface pressure distributions, $P_\infty / P_{t,j} = 0.024$.

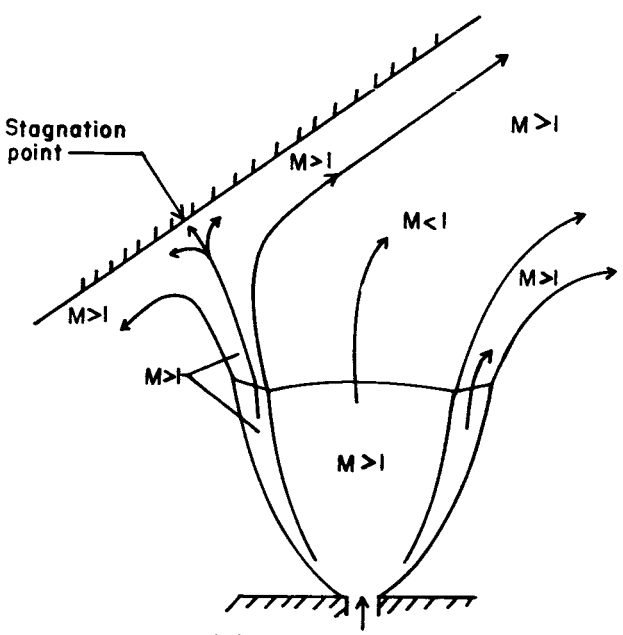

(c) Simplified flow field.

Fig. 11 Characteristics of flow field of sonic jet exhausting against flat plate. $\theta \neq 0°$.

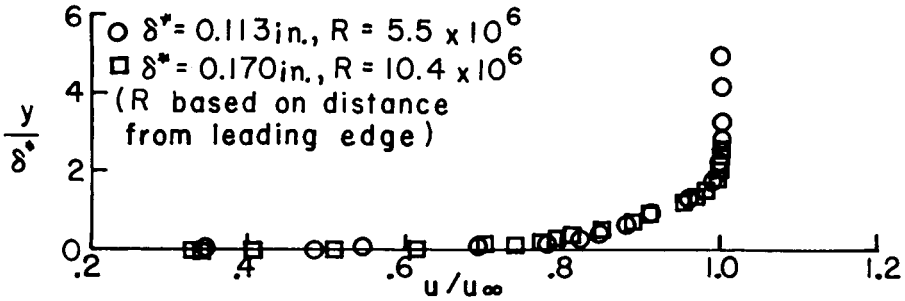

Fig. 12 Boundary layer velocity profiles on plate with roughness. $R_\infty = 8.1 \times 10^6$/ft. ($26.5 \times 10^6$/cm.). $M_\infty = 6.0$.

(a) Reproduction of fig. 14, ref. 4.

(b) Schlieren photograph, $P_{t,j}/P_{t,\infty} = 0.68$, $M_j = 1.0$.

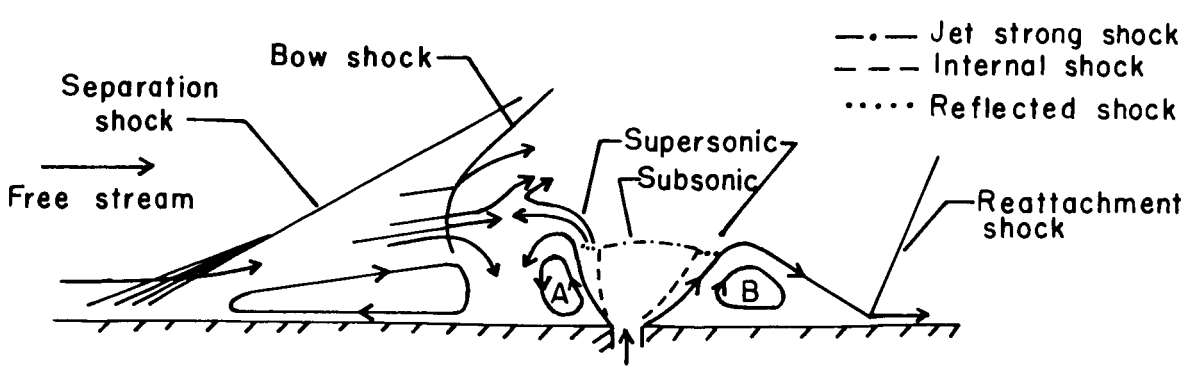

(c) Schematic of flow.

Fig. 13 Example of flow fields with underexpanded jets. $M_\infty = 6.0$.

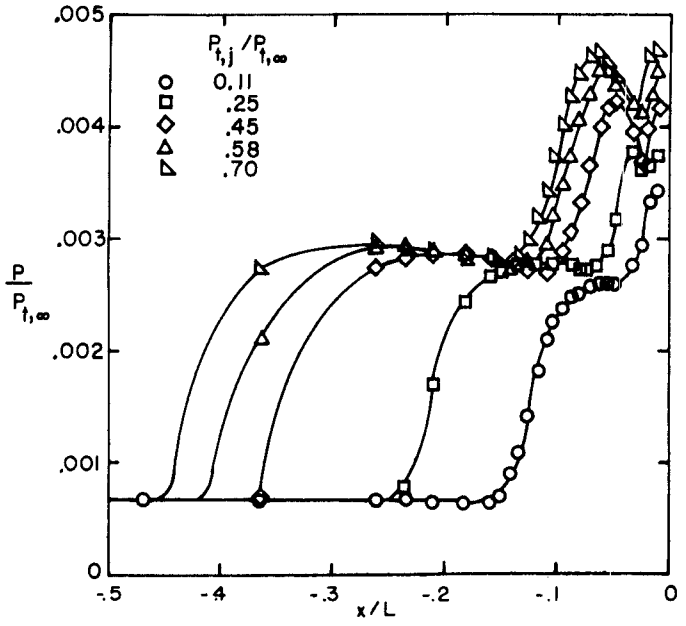

(a) $M_j = 1.0$, d ≠ 0.024 in. (0.061 cm.).

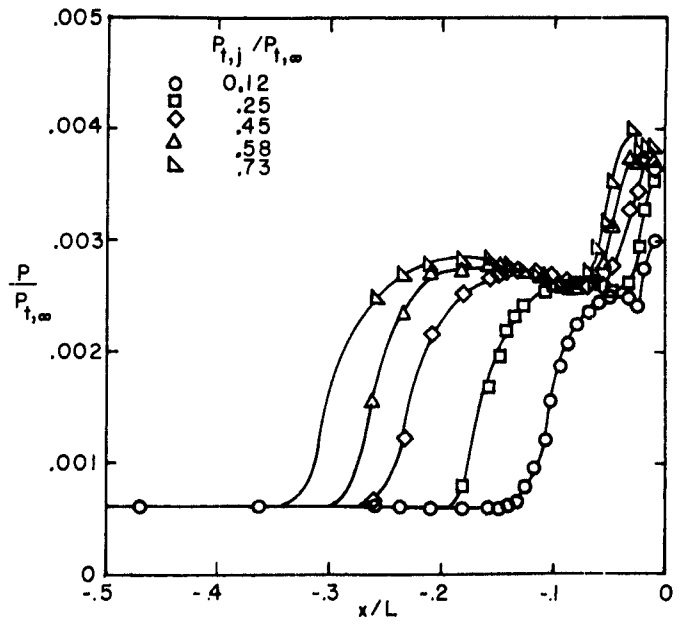

(b) $M_j = 3.2$, d ≠ 0.020 in. (0.051 cm.).

Fig. 14 Chordwise pressure distribution ahead of a jet for varying pressure ratio and various jet exit Mach numbers. $M_\infty = 6.0$.

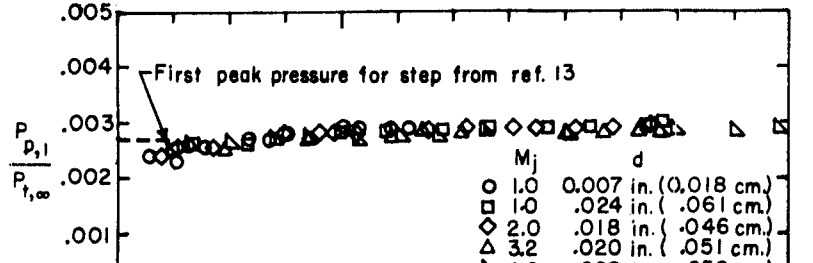

Fig. 15 First peak pressures in separated region.

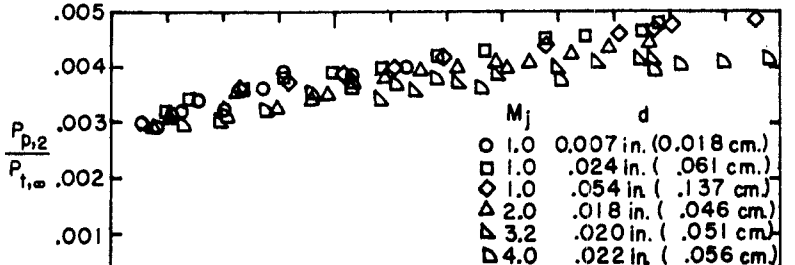

Fig. 16 Second peak pressures in separated region.

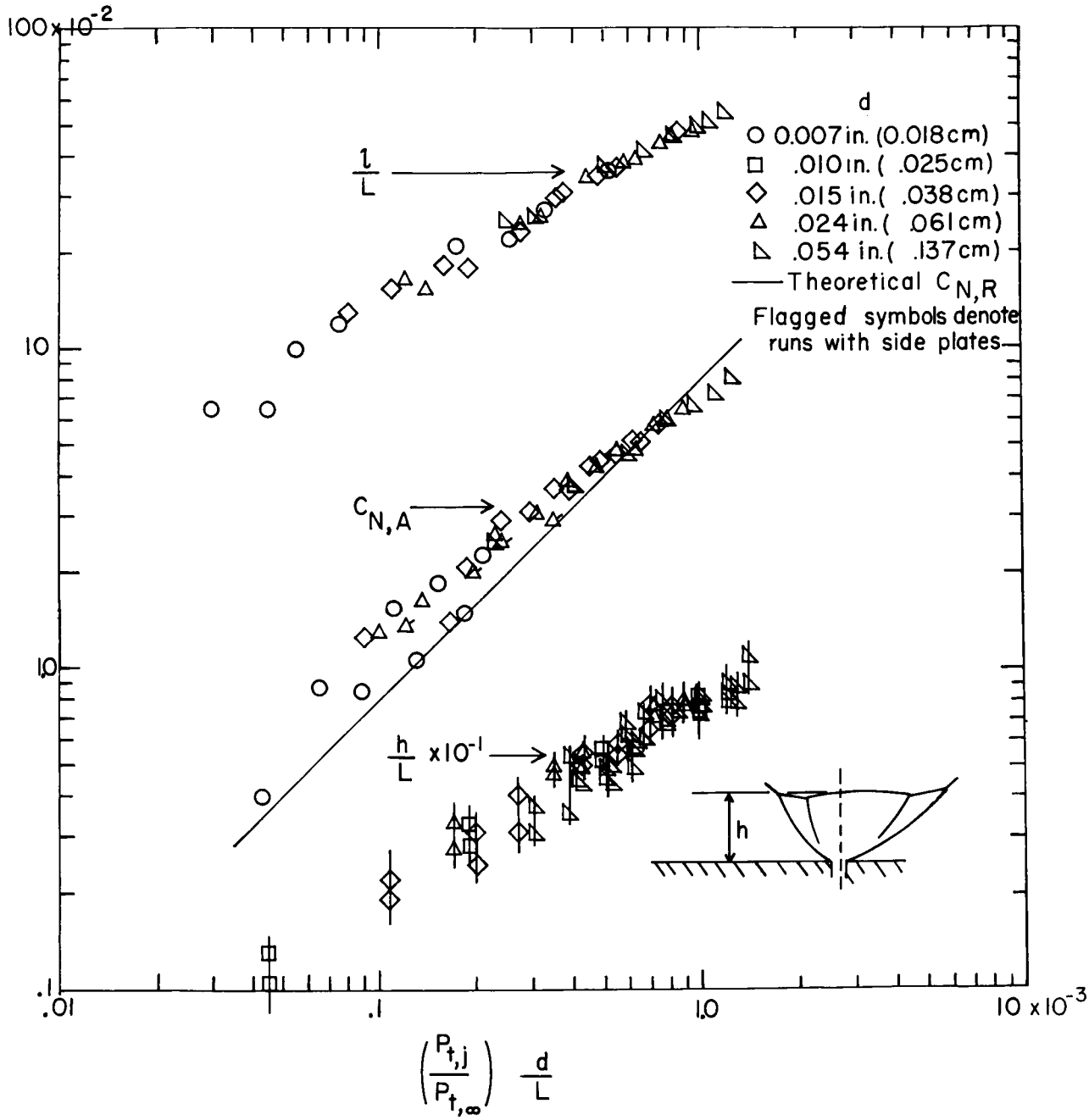

Fig. 17 Comparison of effect of jet mass flow on jet-induced separation distance, aerodynamic normal force and jet strong shock height, various slot widths, $M_j = 1.0$.

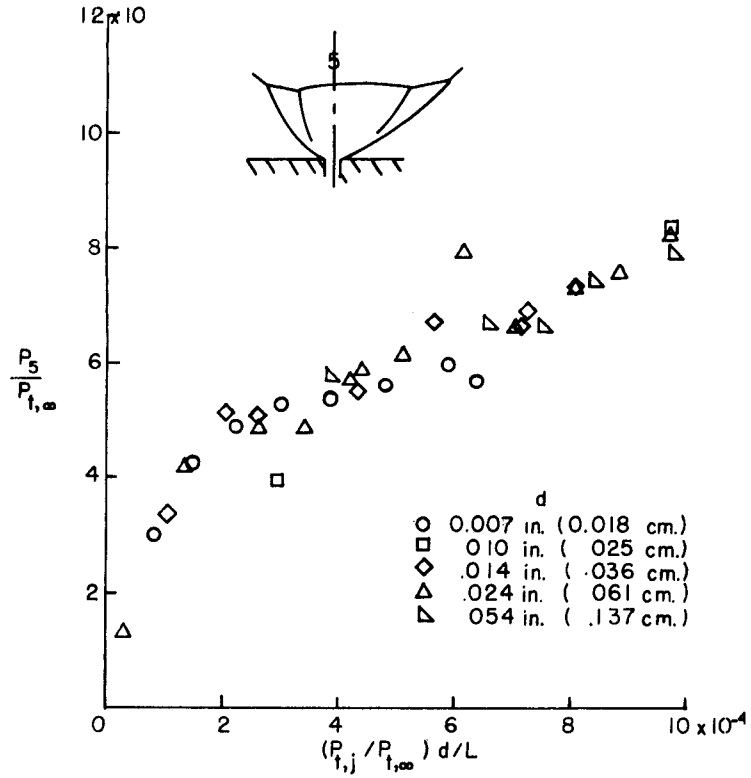

Fig. 18 Static pressures behind jet strong shock. $M_j = 1.0$.

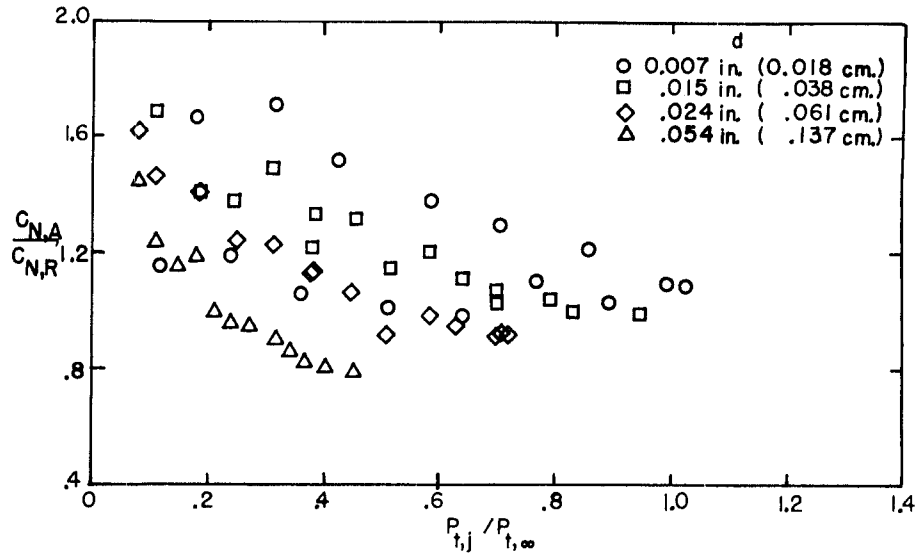

(a) Effect of jet pressure ratio on aerodynamic to reaction normal force coefficient ratio.

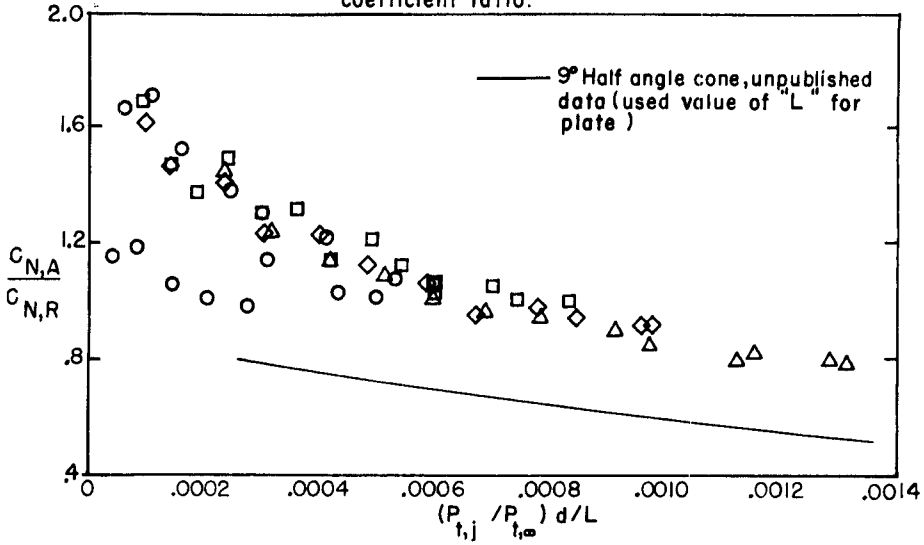

(b) Effect of jet mass flow on aerodynamic to reaction normal force coefficient ratio.

Fig. 19 Effect of various jet parameters on aerodynamic to reaction normal force coefficient ratio; $M_j = 1.0$.

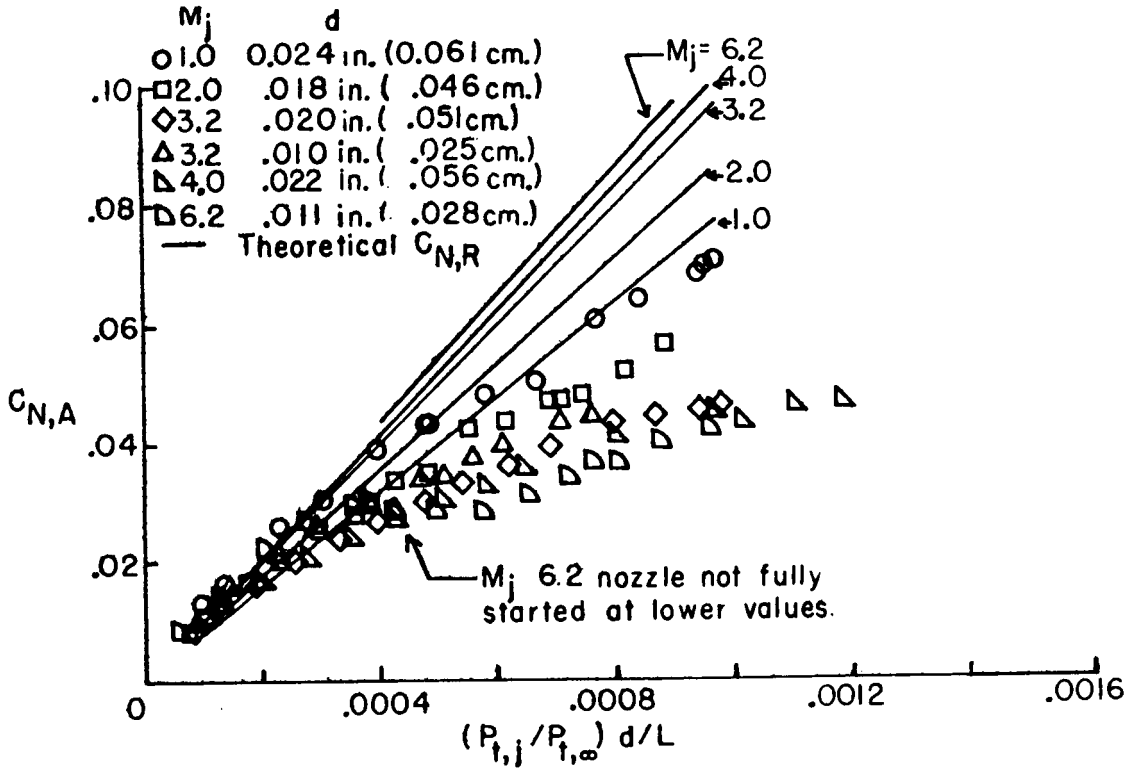

Fig. 20 Effect of jet mass flow on aerodynamic interaction normal force for various Mach numbers.

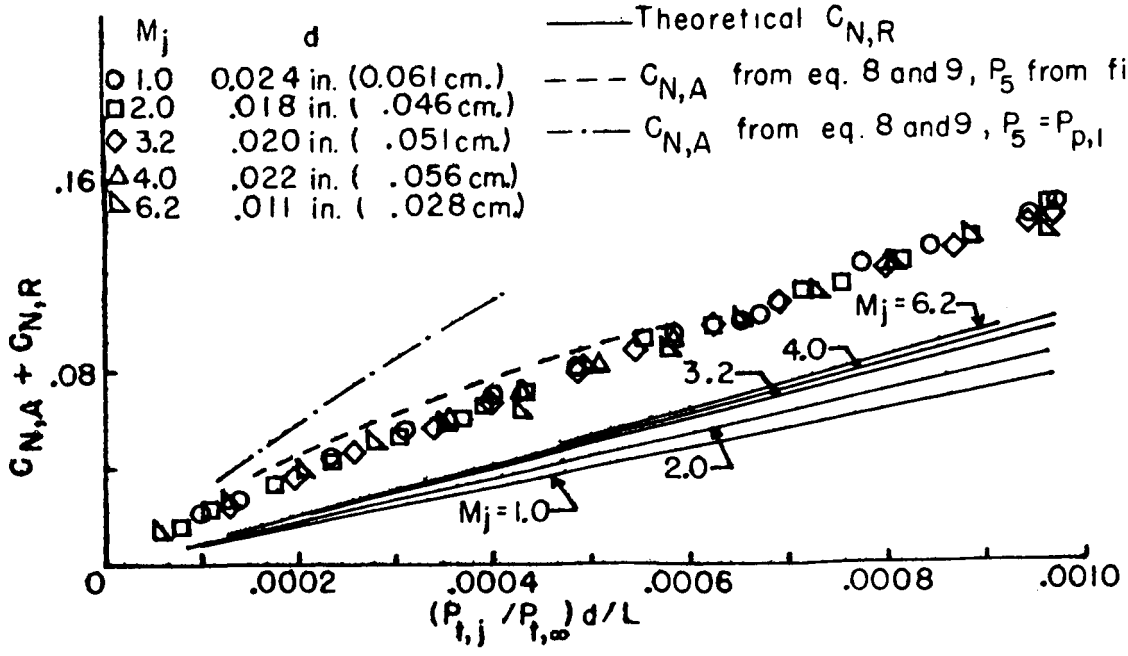

Fig. 21 Effect of jet mass flow on total normal force for various jet Mach numbers.

NASA-Langley, 1966